China Geology 7 (2024) 303−314

China Geology

Journal homepage: http://chinageology.cgs.cn
https://www.sciencedirect.com/journal/china-geology

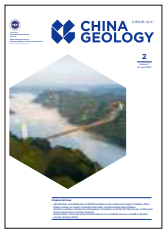

Exploring mechanism of hidden, steep obliquely inclined bedding landslides using a 3DEC model: A case study of the Shanyang landslide in Shaanxi Province, China

Jia-yun Wang[a], Zi-long Wu[b,*], Xiao-ya Shi[a,*], Long-wei Yang[c], Rui-ping Liu[a], Na Lu[a]

[a] *Xi'an Center of China Geological Survey/ Northwest China Center for Geoscience Innovation*, *Xi'an* 710119, *China*
[b] *Xi'an University of Science and Technology*, *Xi'an* 710054, *China*
[c] *Wuhan Design & Research Institute Co., Ltd. of China Coal Technology & Engineering Group*, *Wuhan* 430064, *China*

ARTICLE INFO

Article history:
Received 16 March 2024
Received in revised form 21 April 2024
Accepted 23 April 2024
Available online 25 April 2024

Keywords:
Landslide
Steep obliquely inclined bedding slope
Failure mode
Failure mechanism
Apparent dip creep-buckling
Lateral friction
3DEC model
Landslide numerical model
Geological hazards survey engineering

ABSTRACT

Catastrophic geological disasters frequently occur on slopes with obliquely inclined bedding structures (also referred to as obliquely inclined bedding slopes), where the apparent dip sliding is not readily visible. This phenomenon has become a focal point in landslide research. Yet, there is a lack of studies on the failure modes and mechanisms of hidden, steep obliquely inclined bedding slopes. This study investigated the Shanyang landslide in Shaanxi Province, China. Using field investigations, laboratory tests of geotechnical parameters, and the 3DEC software, this study developed a numerical model of the landslide to analyze the failure process of such slopes. The findings indicate that the Shanyang landslide primarily crept along a weak interlayer under the action of gravity. The landslide, initially following a dip angle with the support of a stable inclined rock mass, shifted direction under the influence of argillization in the weak interlayer, moving towards the apparent dip angle. The slide resistance effect of the karstic dissolution zone was increasingly significant during this process, with lateral friction being the primary resistance force. A reduction in the lateral friction due to karstic dissolution made the apparent dip sliding characteristics of the Shanyang landslide more pronounced. Notably, deformations such as bending and uplift at the slope's foot suggest that the main slide resistance shifts from lateral friction within the karstic dissolution zone to the slope foot's resistance force, leading to the eventual buckling failure of the landslide. This study unveils a novel failure mode of apparent dip creep-buckling in the Shanyang landslide, highlighting the critical role of lateral friction from the karstic dissolution zone in its failure mechanism. These insights offer a valuable reference for mitigating risks and preventing disasters related to obliquely inclined bedding landslides.

1. Introduction

Economic growth, human engineering endeavors, and global climate change have led to increased frequency of large-scale landslides and escalated economic loss and casualties (AU SWC, 1998; Schuster RL and Lynn MH, 2001; Huang RQ, 2007; Yin Y et al., 2023). Obliquely inclined bedding slopes with less visible apparent dip sliding are prone to undergo catastrophic geological events, making them a focal point in landslide research. These rock slopes, characterized by their obliquely inclined bedding structures, are notably common in carbonate regions in southwestern China (Yin YP, 2008). A handful of scholars have delved into the characteristics and mechanisms behind these landslides. Liu CZ et al (1995) introduced the concept of "apparent sliding force" following an analysis of the deformation mechanisms of the hazardous Lianzi cliff rock mass along the Yangtze River, laying the theoretical groundwork for understanding the apparent dip sliding in obliquely inclined bedding rock slopes. Yin YP (2010) and Yin YP et al. (2011) proposed a failure mode for these slopes and conducted a thorough investigation into the failure mechanisms of the Jiweishan landslide in Wulong. Building on these studies, they identified the conditions conducive to the apparent dip sliding of an obliquely inclined bedding landslide.

On August 12, 2015, Shanyang, Shaanxi Province, China, witnessed a landslide involving 1.68×10^6 m^3 of materials

First author: *E-mail address*: wjiayun@mail.cgs.gov.cn (Jia-yun Wang).

* Corresponding author: *E-mail address*: xustwzl@163.com (Zi-long Wu); 627892564@qq.com (Xiao-ya Shi).

Literary editor: Li-qiong Jia
doi:10.31035/cg2024044
2096-5192/© 2024 China Geology Editorial Office.

("8.12" landslide; Fig. 1). This event, occurring on a hidden, steep obliquely inclined bedding slope, led to 65 fatalities and nearly 0.5×10^9 RMB in economic loss. Yet, research into the failure modes and mechanisms of hidden, steep obliquely inclined bedding slopes remains limited. The dip angle of the potential sliding surface in the slope is greater than the slope angle, so it is hidden below the foot of the slope to form the "hidden type" slope and the large landslides with "creep (bending) - shearing" mode (creep-buckling mode) controlled by soft layers are prone to develop (Huang RQ, 2007). The apparent bedding orientation and the slide resistance at the slope's base were key factors in this disaster. Buckling failure, a common failure mode for such slopes, has attracted significant research interest. Kutte HK and Müller L (1981) initially proposed the concept of buckling failure and developed an ultimate load formula for it on bedding rock slopes. Sun GZ and Zhang WB (1985) and Sun GZ (1988) advanced this work by creating a geomechanical model for landslides prone to buckling, incorporating the structural characteristics of the rock masses and the geological settings of bedding rock slopes, and further refined the ultimate load formula. Thorough research has been conducted on the geomechanical model and instability criteria for buckling failure in bedding rock slopes, laying a solid foundation for understanding this phenomenon (Xu B et al., 2022; Mu JQ et al., 2022; Qiu P et al., 2023; Wang R et al., 2023; Yang C et al., 2023). Building upon these studies, researchers have explored the characteristics, contributing factors, and mechanisms of buckling failure in bedding rock slopes through formula derivation, physical simulations, and numerical modeling (Yin Y et al., 2017; Zou Z et al., 2017; Yan GQ et al., 2019; Yang L et al., 2020; Pipatpongsa T et al., 2022; Xiong X et al., 2022; Rahman AU et al., 2023; Zhang Y et al., 2023; Cui F et al., 2021). However, these studies primarily address buckling failure of bedding landslides, with scant attention to the failure modes or mechanisms of hidden steep obliquely inclined bedding landslides. The failure mode of the Shanyang landslide, with its distinct hidden steep obliquely inclined bedding structures, diverges from the buckling observed in bedding landslides and the apparent dip sliding of obliquely inclined bedding landslides (Wang J et al., 2019). To elucidate the failure mechanisms of hidden, steep obliquely inclined bedding landslides, this study, leveraging field surveys, geotechnical parameter laboratory tests, and 3DEC software, constructed a numerical model of the Shanyang landslide to simulate and analyze the failure process. The findings of this study will offer insights into the risk mitigation and prevention of obliquely inclined bedding landslides.

2. Geological setting

The Shanyang landslide region, situated within a monsoon subhumid climate zone, experiences annual rainfall ranging between 700 mm and 900 mm, with an average of 709 mm. Precipitation distribution throughout the year is notably uneven, with the bulk of rainfall, accounting for over 50% of the annual total, occurring from July to September,

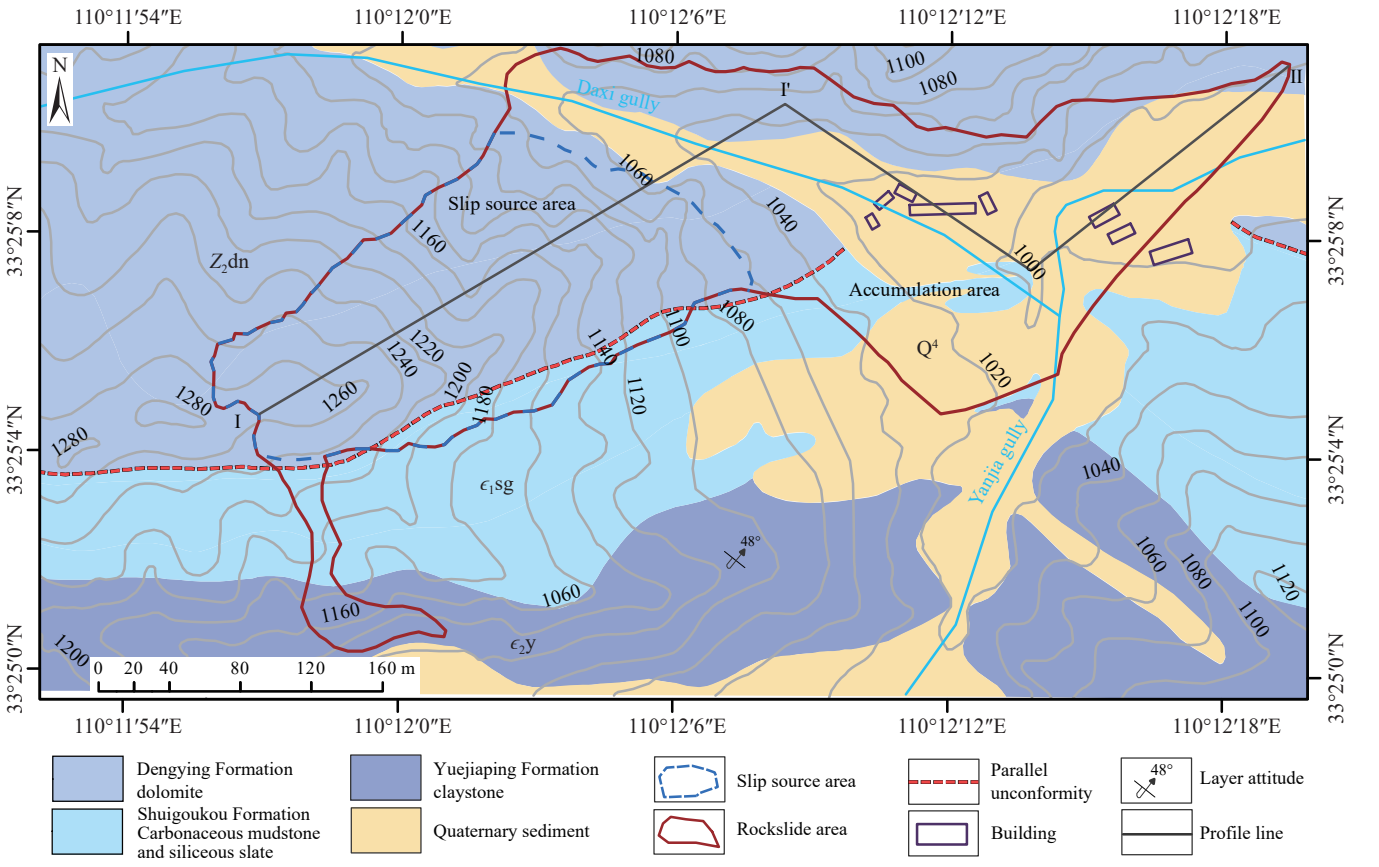

Fig. 1. Plan map of the Shanyang landslide.

predominantly as heavy showers.

The "8.12" landslide occurred on a steep bedrock mountain slope with a 38° overall gradient and three free faces, overlooking the V-shaped Daxi gully and forming a steeply dipping oblique slope. The mountain slope where the landslide originated exhibits elevations ranging between 1025 m and 1300 m, while the front of the accumulation zone has an elevation of 970 m, resulting in a vertical drop of up to 330 m from the mountain slope's top to the front of the accumulation zone. This landslide is situated within the thin-skinned thrust nappe structural belt in southern Qinling and on the southern flank of the Yaolinghe anticlinorium. The stratigraphic sequence here is overturned, with the thick and very thick dolomite layers at attitudes of 345°–20°∠43°–60° in the Sinian Dengying Formation (Z_2dn) overlying the weak carbonaceous mudstones and siliceous slates at attitudes of 340°–20°∠32°–56° in the Cambrian Shuigoukou Formation ($Є_1sg$), forming a slope structure with a hard upper part and a weak lower part.

The Daxi gully and Yanjia gully intersect at the landslide's front, where there is no surface runoff. Rainwater infiltrates rock masses through joint fractures and karstic dissolution channels, recharging the groundwater. The groundwater accumulates on the surface of the underlying weak interlayer, eroding and weakening it. Consequently, shear displacement occurred within the weak interlayer, leading to the landslide's creep along the weak interlayer.

3. Sliding rock mass' structure and landslide's characteristics

3.1. Structure of sliding rock mass

Due to the monoclinal structure and overturned strata, rock layers, inclining sharply towards NE, intersect the slope's frontal free face at an angle, resulting in the formation of the distinct steep obliquely inclined rock slope. Based on the topographic data before the landslide occurring, the elevation data along the cross-sectional line is extracted by ArcGIS software. The data extracted by ArcGIS software is imported into Grapher software combined with geologic map information and the cross-sectional map is generated (Fig. 2). Beneath the hard dolomites at an attitude of 15°∠43° lies weak carbonaceous mudstones and siliceous slates at an attitude of 15°∠48°, with the weak surface becoming a potential slip surface for the landslide. The sliding mass crept along this weak surface following the true dip angle but was halted by the inclined stable bedrock in the west, causing the slip direction to shift from a true dip angle of NNE15° to an apparent dip angle of NEE60°. The apparent dip angle for the weak carbonaceous mudstones and siliceous slates stands at 38.12°, almost mirroring the slope's inclination (38°), making the potential slip surface hidden underground and forming a hidden slope. Thus, the slope is classified as a hidden, steep obliquely inclined bedding slope governed by the underlying weak interlayer.

The Shanyang landslide occurred on a hidden, steep obliquely inclined bedding slope, governed by the underlying weak interlayer. The hidden bedding landslides of this type typically exhibit a "creep (bending)-shear" failure mode dictated by weak interlayers. Huang RQ (2007) categorized a slope's failure mode into two segments from a mechanical perspective: The upper and middle bedding section, which constitute the "driving area" where creep occurs, and the lower section, where bending uplift occurs, referred to as the "passive area". Due to gravitational forces, the rock mass in the "driving area" slides along the weak interlayer, while compression in the "passive area" leads to bending uplift deformation of the rock mass in this area. This deformation intensifies until bending-shear (buckling) failure ensues, triggering a landslide. The slope hosting the Shanyang landslide mirrors the structural pattern mentioned above.

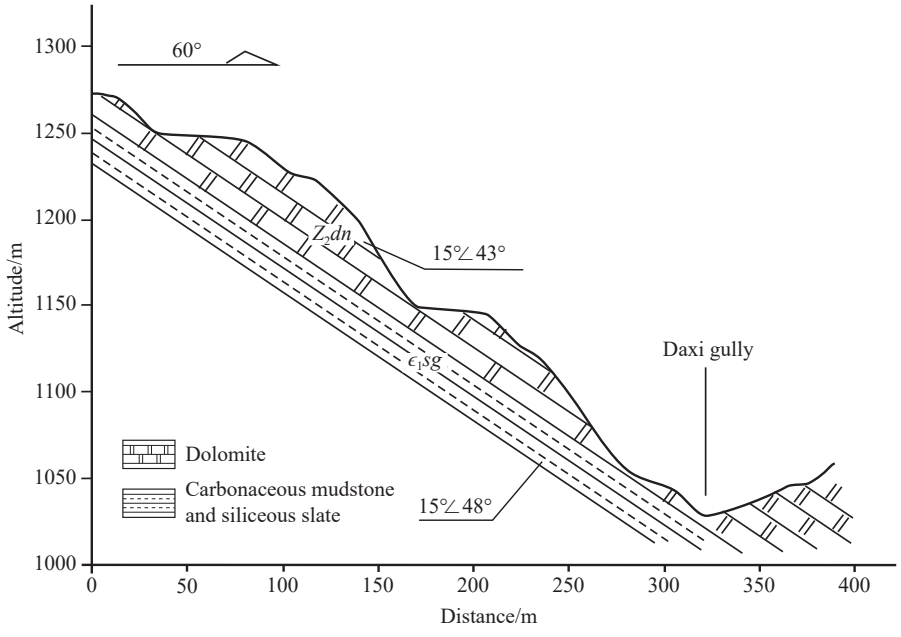

Fig. 2. Slope structure of Shanyang landslide (I-I').

Specifically, it has a prismatic body governed by structural planes prior to sliding. This prismatic structure, corresponding to the landslide's anatomy, is divided into "a driving rock mass" and "a slide-resisting rock mass" based on their roles in the sliding process.

3.2. Characteristics of structural planes

The Shanyang landslide's sliding rock mass was separated from the mountain slope by three key structural planes (Fig. 3): The parallel unconformity T0 (15°∠48°) between the dolomites and the underlying weaker carbonaceous mudstones and siliceous slates, the karstic dissolution structural plane T1 (113°∠76°) located to the west of the landslide, and the steeply inclined unloading joint discontinuity T2 (275°∠66°). A stereographic projection sketch reveals that the intersection line between T0 and T1 closely aligns with the landslide's sliding direction, with a dip angle slightly exceeding the slope's gradient, making them the primary structural planes controlling the landslide. Conversely, the intersection line between T0 and T2 nearly perpendicularly intersects the landslide's sliding path, whereas the T1 and T2 intersection line is almost opposite to the sliding direction, effectively segmenting the sliding rock mass. Consequently, the parallel unconformity T0 serves as both the principal slip surface and the right boundary of the landslide. The karstic dissolution structural plane T1 defines the left boundary, and the steeply inclined unloading joint discontinuity T2 segments the landslide.

3.3. Characteristics of slip surface and shear outlet

The landslide's slip surface is obscured by the sliding rock mass, except for its central and rear portions, which are exposed integrally. Both portions appear undulating and smooth, lacking distinct sliding striations or prominent antistep features (Fig. 4a). The sliding-zone soils, composed of unconsolidated mud resulting from interlayer shear, measure about 5 cm in thickness. This suggests that significant interlayer shear, driven by the gravitational pull of the mountain slope and groundwater, transforms the weak interlayer into mud (Fig. 4b), facilitating the landslide's prolonged bedding creep along the weak interlayer in the true dip direction. The shear outlet, concealed by the landslide mass and the talus at the landslide's rear, is estimated to be approximately 22 m above the slope's toe in the gully, as deduced from the landslide's original and current terrains and the parallel unconformity. The deformation features around the shear outlet are pronounced, with intense tensile deformations observed to the left and notable bending and uplift deformation emerging within the remaining rock mass to the right (Fig. 4c). These deformations suggest the presence of buckling failure at the shear outlet, contrasting sharply with the shear slip striations caused by apparent dip sliding in the

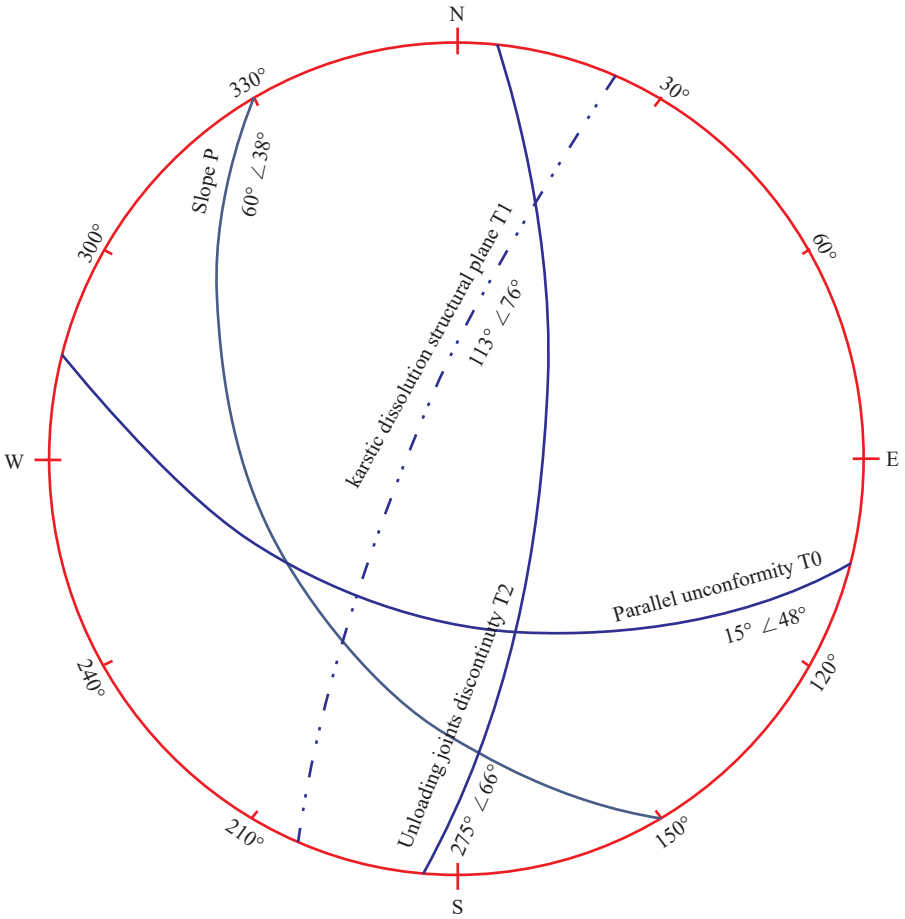

Fig. 3. Three groups of joints stereographic projection.

Fig. 4. Characteristics of the slip surface and shearing outlet. a–antistep in the slip surface; b–mud compounds in weak intercalation; c–bending deformation in outlet.

landslide's central and rear portions. The Shanyang landslide exited the hillside along the apparent dip angle, colliding twice with valley slopes, achieving a maximum travel distance of about 600 m and an estimated exit speed of 74.16 m/s, indicating a high-speed, long-runout landslide. The movement process can be segmented into four zones (Fig. 5): The apparent dip creep-buckling zone, the main accumulation zone, the landslide collision zone, and the fragment flow zone (Wang JY et al., 2018). Based on the topographic data before and after the landslide occurring, the profile of movement zones is generated combined with field investigation by means of ArcGIS extraction of elevation data and Grapher mapping (Fig. 6). The apparent dip creep-buckling zone, situated in the landslide's source area, transformed the landslide from the true dip angle to the apparent dip angle. The main accumulation zone spans from the shear outlet to the first collision point (first collision) on Daxi gully's north slope along the apparent dip angle. The collision accumulation zone extends from the first collision point to the second collision point on Yanjia gully's east slope, following a SSE145° trajectory. Lastly, the debris flow zone covers the area from the second collision point to the front of the landslide debris, composed of fragmented materials.

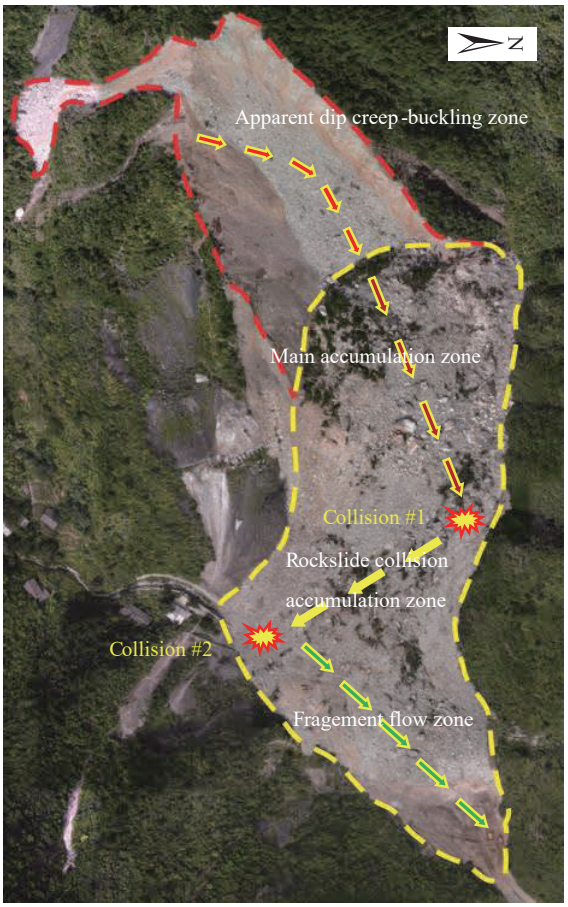

Fig. 5. Plane view of movement zones.

4. Failure process simulation of Shanyang landslide

Computer modeling finds wide application in the analysis and evaluation of landslide stability (Cundall PA and Hart RD, 1985; Sassa K, 1988; Hungr O and McDougall S, 2009; Pastor M et al., 2009). The distinct element method has emerged as a pivotal numerical modeling tool for simulating the failure of rock slopes with intricate structural features such as bedding planes, fissures, and joints. In the early 1970s, Cundall PA (1971, 1980) introduced the concept of the distinct element method to examine the movement processes and characteristics of rock slopes. Subsequently, in the early 1980s, Cundall developed the universal distinct element code (UDEC), which employs the Mohr-Coulomb yield criterion to investigate rock mass failure. In 1986, in collaboration with the Itasca Consulting Group Inc., Cundall advanced the three-dimensional distinct element code (3DEC). Since its introduction, 3DEC has been extensively applied in numerical simulations of the mechanical behavior of rock masses, particularly focusing on large strain deformations and planar rotational slides.

4.1. Modeling of Shanyang landslide

This study investigated the failure process of the Shanyang landslide using 3DEC modeling software. By examining the geological structures and the characteristics of structural plane combination of the Shanyang landslide, this study created a 3DEC model with dimensions of 425 m in length, 257 m in width, and 170 m in height. Within 3DEC, the model was segmented into different zones representing the two bedding rock masses, parallel unconformities, and karstic dissolution structural plane, with each zone further divided into trihedral groups using the software's algorithms. The simulation of the rock mass failure process utilized the Mohr-Coulomb yield criterion and the ubiquitous-Joint model. The strength index for the dolomites were determined through physical test, compression test, deformation test and triaxial

strength tests in Xi'an University of Technology laboratory (Table 1), while the weakening joint strength was calculated using the Hoek-Brown strength criterion. The strength indices for the carbonaceous mudstones and siliceous slates were derived from empirical data (Table 2). The dissolution rate in the karstic dissolution zone of the Shanyang landslide is 44.8%, leading to the zone's strength parameters calculated at 55.2% of the dolomites' strength. The long-term strength of the carbonaceous mudstones is 0.8 times their natural strength, and the argillization strength of the weak interlayer is 0.6 times its natural strength. Utilizing 3DEC, this study simulated three processes including the creep caused by gravity, the sliding with the argillization of the weak interlayer, and the buckling failure due to the reduced lateral friction force in the karstic dissolution zone. Furthermore, observation points No. 1, 2, 3, and 4 were set up at the top of the sliding mass, along the karstic dissolution structural plane, and at the toe of the sliding mass to monitor displacements across different sections of the landslide.

4.2. Simulation of landslide creep due to gravity

This study simulated the landslide creep, due to gravity, along the weak interlayer T0 with the gradual argillization of the interlayer shear. Fig. 7 illustrates that the peak displacement occurred at the top right side of the landslide, with creep displacement decreasing progressively from this point towards the karstic dissolution zone and the mountain slope's toe, hindered by the inclined stable rock mass barrier and the resistance from the slide-resisting rock mass. The complete displacement *vs.* time-step process curve of Shanyang landslide in *X*, *Y* and *Z* directions are shown in Figs. 8, 9 and Fig. 10, respectively. Analyzing the displacement *vs.* time step curves (0–36258 step) for monitoring points in both the *X* and *Y* directions, as shown in Figs. 8–9, reveals that the displacements at points #1 and #2

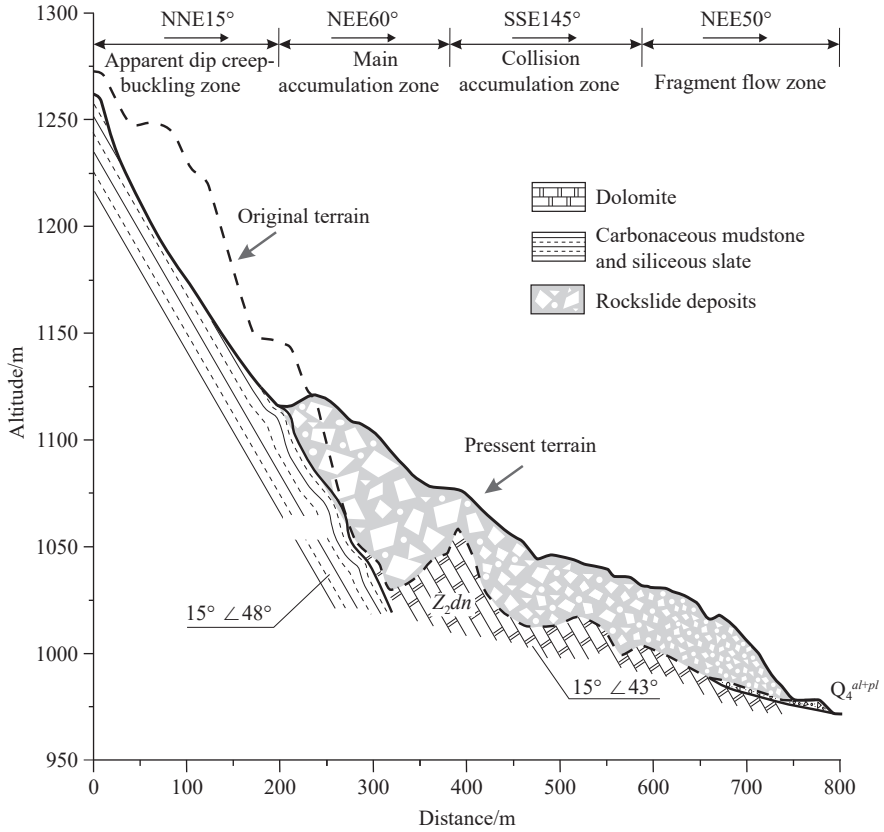

Fig. 6. Profile of movement zones.

Table 1. Physical and mechanic parameters of the Shanyang landslide.

Rock type	Volume weight /(kg/m^3)	Elastic modulus /GPa	Poisson ratio	Cohesion /MPa	Internal friction angle /°
Dengying dolomite	2830	59	0.2	12.85	48.53
Shuigoukou mudstone and siliceous slate	2700	17.3	0.25	19.5	32.8

Table 2. Physical and mechanic parameters of weak layers in the Shanyang landslide.

Weak layer type	Internal friction angle /°	Cohesion /MPa	Normal stiffness /(GPa/m)	Tangential stiffness /(GPa/m)
Weak interlayer T0	19.38	0.06	9	9
Karst dissolution zone T1	26.79	7.09	9	9
Steeply inclined unloading joints	34	0.6	9	9

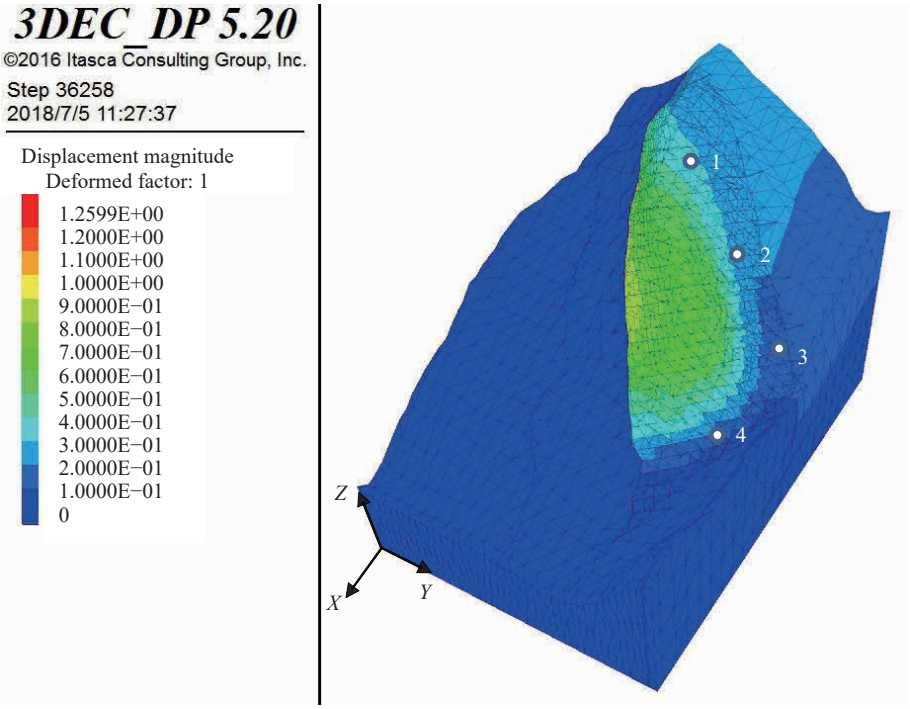

Fig. 7. Contour map showing the creep displacement of the landslide under the gravity.

in the *Y*-direction significantly exceeded those in the *X*-direction. Conversely, the displacements at points #3 and #4 in the *X*-direction surpassed those in the *Y*-direction. These results indicate that the central and rear portions of the driving rock mass underwent bedding sliding along the weak interlayer and its front exhibited a trend towards apparent dip sliding due to the obstruction posed by the inclined stable rock mass and the compression from the creeping driving rock mass. Furthermore, the front of the driving rock mass exhibits a more pronounced tendency to creep in the apparent dip direction than the slide-resisting rock mass.

4.3. Simulation of landslide sliding under argillization of the weak interlayer

This study simulated the deformations and sliding of the landslide, influenced by the argillization of the weak interlayer and the penetration along the central and rear portions of the slip surface, as well as the bedding creep of the driving rock mass. The argillization strength of the weak interlayer is 0.6 times its natural strength, and argillization strength parameters c = 45 kPa and φ = 14.53° were used as the weak interlayer's mechanical parameters. Fig. 11 illustrates that the overall deformation and sliding trends of the landslide, due to the argillization of the weak interlayer, resembled those caused by gravity. However, the sliding displacements significantly exceeded the creep displacements. Data from Fig. 7 and Fig. 11 reveal that the maximum displacement during this deformation and sliding was over twice that caused by gravity alone. Analyzing the displacement *vs.* time step curves (36259–46669 step) for monitoring points in both the *X* and *Y* directions, as shown in Fig. 8 and Fig. 9, shows that the displacements in the *X*-direction and their rise rates at points #3 and #4 were markedly greater than those at points #1 and #2, and that the

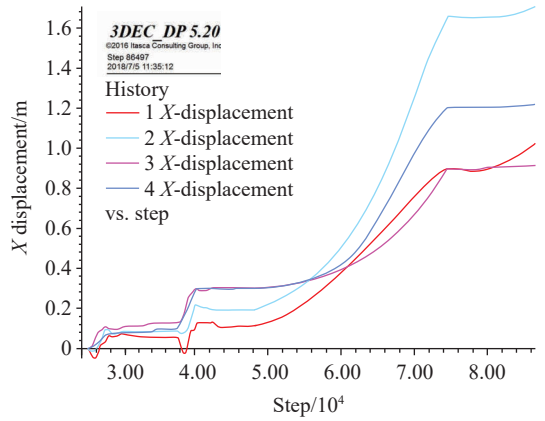

Fig. 8. Displacement *vs.* time step curves of monitoring points in *X*-direction.

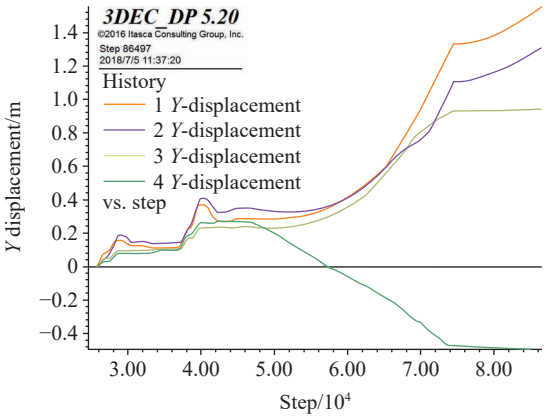

Fig. 9. Displacement *vs.* time step curves of monitoring points in *Y*-direction.

displacements in the *Y*-direction and their rise rates at points #1 and #2 significantly exceeded those at points #3 and #4. Comparing the displacement *vs.* time step curves (36259–46669 step) for the monitoring points, as shown in Fig. 8 and Fig. 9, reveals that, at points #1 and #2, the displacements in the *Y*-direction were considerably greater than those in the *X*-direction. In contrast, at points #3 and #4, the displacements in the *X*-direction significantly surpassed that in the *Y*-direction. These findings reflect the bedding sliding of the driving rock mass along the weak interlayer, the apparent dip sliding of the driving mass along the karstic dissolution zone, and the apparent dip sliding of the slide-resisting rock mass. Table 3 confirms that the displacement of the landslide, influenced by the argillization of the weak interlayer, substantially exceeded that caused by gravity, highlighting the pronounced characteristics of bedding slide along the weak interlayer and the apparent dip sliding of the landslide under these simulation conditions.

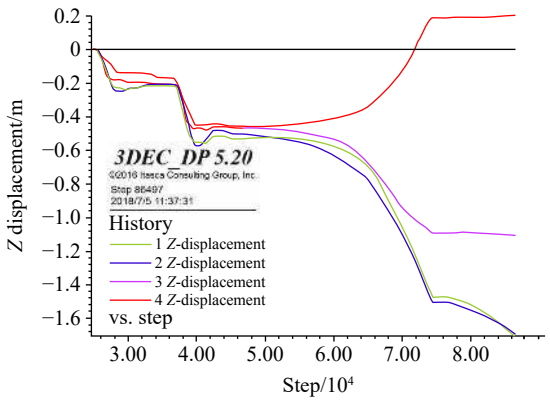

Fig. 10. Displacement *vs.* time step curves of monitoring points in *Z*-direction.

4.4. Simulation of buckling failure triggered by karstic dissolution-induced reduction in lateral friction force

This study simulated the buckling deformation and failure of the slide-resisting rock mass due to compression from the apparent dip sliding of the driving rock mass, triggered by a karstic dissolution-induced reduction in the rock strength and lateral friction force. Given a dissolution rate of 44.8%, the strength parameters for the karstic dissolution zone were set to 55.2% of dolomite strength, namely c = 7.09 MPa and φ = 26.79°. Fig. 12 reveals that the maximum displacement occurred in the central and rear portions of the landslide, while the minimum displacement emerged at the toe of the mountain slope. This indicates the emergence of the landslide' s overall apparent dip sliding due to reduced lateral friction force. Analyzing the displacement *vs.* time step curves (46670–86497 step) for monitoring points in the *X*, *Y* and *Z* directions, as shown in Figs. 8, 9 and 10, illustrate a sharp increase in landslide displacement under reduced lateral friction compared to the above-mentioned two conditions. Table 4 shows that the displacements in the *Y*-direction at points #1 and #2 in the central and rear portions notably increased by 5.34 times and 3.66 times, respectively those under the argillization of the weak interlayer. Similarly, the displacements in the *Y*-direction at point #3 near the karstic dissolution zone and point #4 at the toe of the mountain slope significantly increased by 3.89 times and 1.82 times, respectively, despite the slide-resistance effect. These displacement data highlight the overall trend towards apparent dip sliding, as well as the slide-resistance characteristics of the karstic dissolution zone and the slide-resisting rock mass, especially the slide-resisting rock mass. Notably, point #4 exhibited abnormal displacement in the *Y* and *Z* directions,

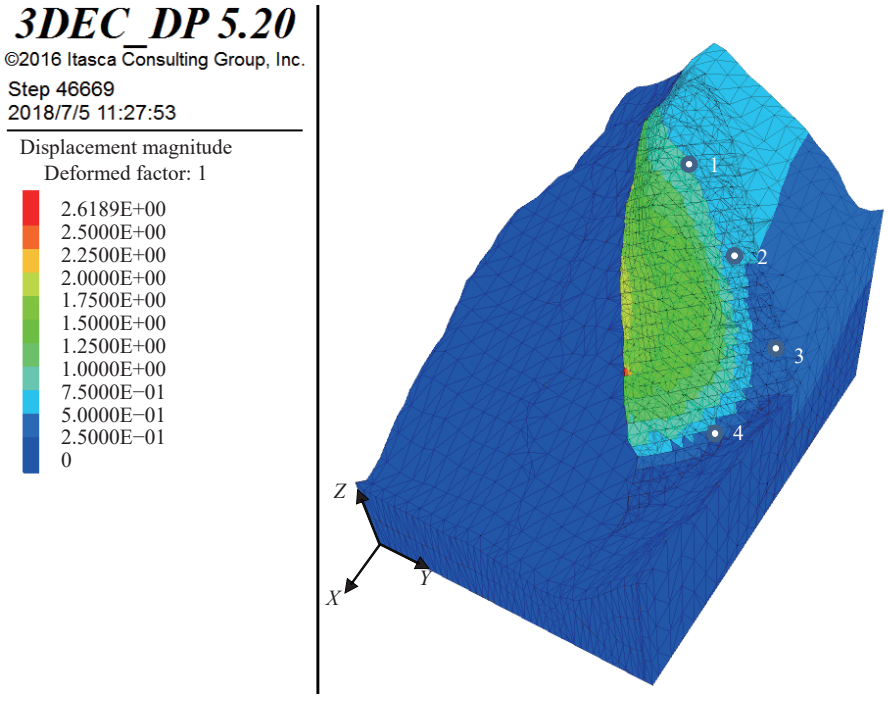

Fig. 11. Contour map showing the landslide displacement.

with synchronous decreases in both directions, underscoring the significant upward and backward sliding trends, as indicated by the displacement *vs.* time step curves and data. This reflects the bending deformations of the slide-resisting rock mass and the deformation trends of the landslide prior to buckling failure (Fig. 13).

5. Discussion

Based on the above analyses, it can be concluded the failure mechanisms of the Shanyang landslide characterized by apparent dip creep-buckling. Initially, interlayer shear led to the progressive argillization of the weak interlayer under the gravitational forces of groundwater and the mountain slope (Fig. 14). This caused a continuous decrease in the shear strength of the weak interlayer and an increase in the sliding force of the landslide mass. Subsequently, the driving rock mass crept along the true dip angle (NNE15°) in a prolonged period, governed by a steep obliquely inclined bedding structure. Due to the presence of an inclined stable rock mass barrier to the west of the landslide, the driving rock mass underwent planar rotation, altering its slide direction from the true dip angle to an apparent dip angle of NNE60°. As the driving rock mass started to creep in the apparent dip direction, the slide-resisting rock mass at the mountain slope's toe was progressively compressed. Then, the lateral friction force diminished gradually with the progression of karstic dissolution dissolution, leading to a swift rise in the sliding force of the landslide mass, ensuing bending deformation of the "slide-resisting rock mass", and eventual buckling failure (Fig. 15). This was accompanied by the brittle failure of the karstic dissolution structural plane between the slide-resisting rock mass and the lateral stable bedrock, causing the overall landslide to slide out of the mountain slope in the apparent dip direction, covering an area of 0.07 km² after two collisions (Fig. 16). The failure processes of the landslide evolved from initial true dip creep to planar rotational creep, culminating in apparent dip creep-buckling failure. Liu CZ et al. (1995) introduced the concept of "apparent sliding force" through their study of the failure mode of the Lianziya unstable rock mass in the Three Gorges area; Yin YP et al. (2011) proposed

Table 3. Displacements in *X* and *Y* directions at monitoring points due to gravity and the argillization of weak interlayer.

Simulated condition	Creep under gravity		Sliding under argillization of weak interlayer	
	X/m	*Y*/m	*X*/m	*Y*/m
Point #1	0.052	0.114	0.114	0.290
Point #2	0.084	0.144	0.194	0.355
Point #3	0.128	0.108	0.304	0.241
Point #4	0.096	0.100	0.301	0.272

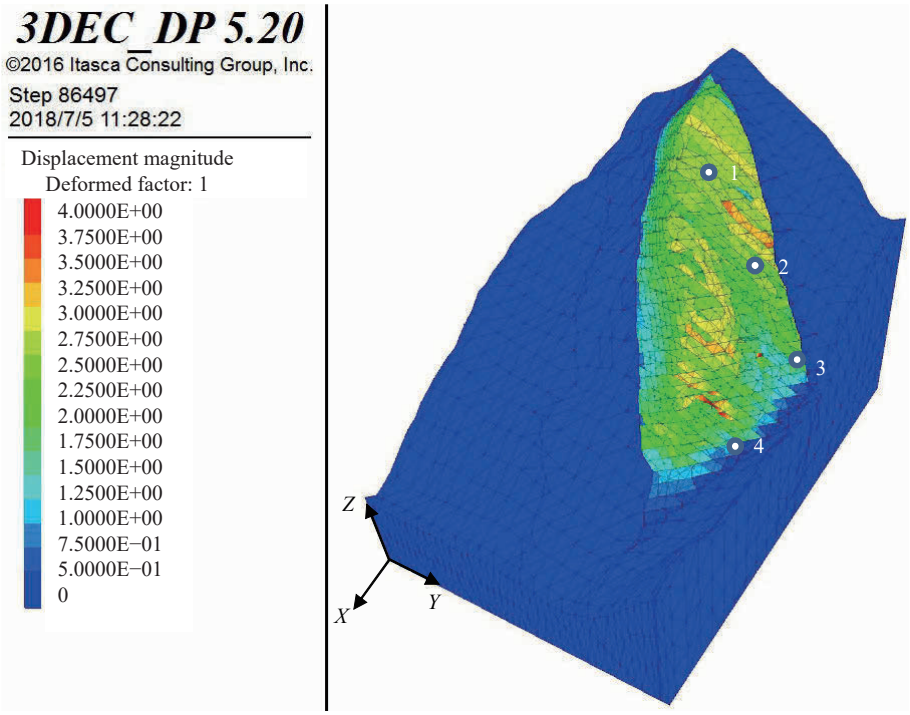

Fig. 12. Contour map showing landslide displacement under the reduction in the lateral friction force of the karstic dissolution.

Table 4. Displacements in *X*, *Y*, and *Z* directions at monitoring points under different conditions.

Simulated condition	Creep under gravity			Slide under argillization of weak interlayer			Buckling failure under karstic dissolution		
	X/m	*Y*/m	*Z*/m	*X*/m	*Y*/m	*Z*/m	*X*/m	*Y*/m	*Z*/m
Point #1	0.052	0.114	−0.218	0.114	0.290	−0.530	1.03	1.55	−1.70
Point #2	0.084	0.144	−0.213	0.194	0.355	−0.501	1.71	1.30	−1.69
Point #3	0.128	0.108	−0.208	0.304	0.241	−0.467	0.914	0.937	−1.10
Point #4	0.096	0.100	−0.170	0.301	0.272	−0.456	1.22	−0.496	0.202

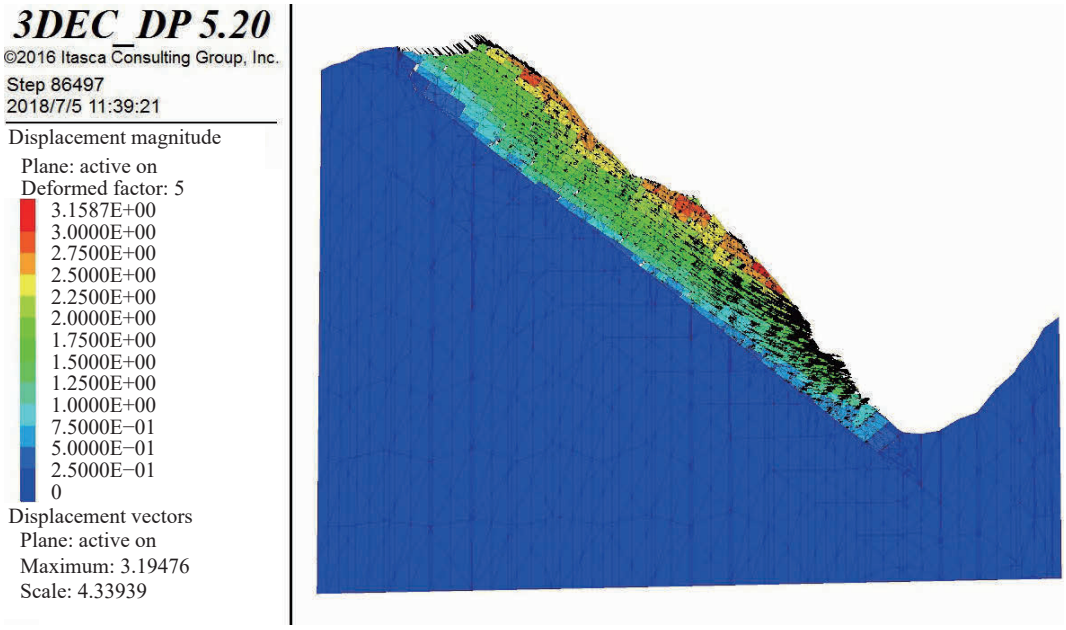

Fig. 13. Contour map showing longitudinal displacement of the landslide before buckling failure.

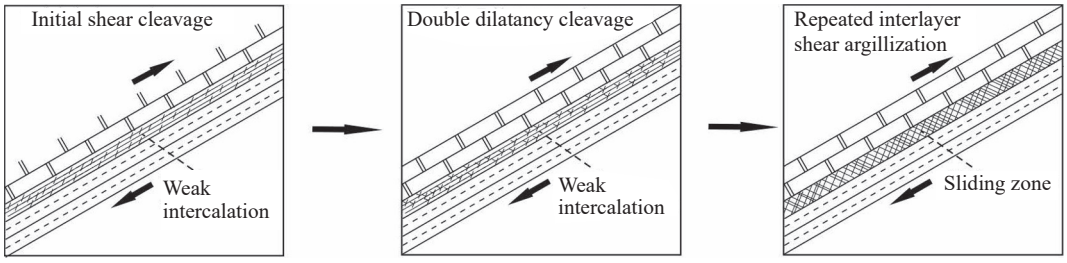

Fig. 14. Evolutionary process of weak interlayer argillization by interlayer shear.

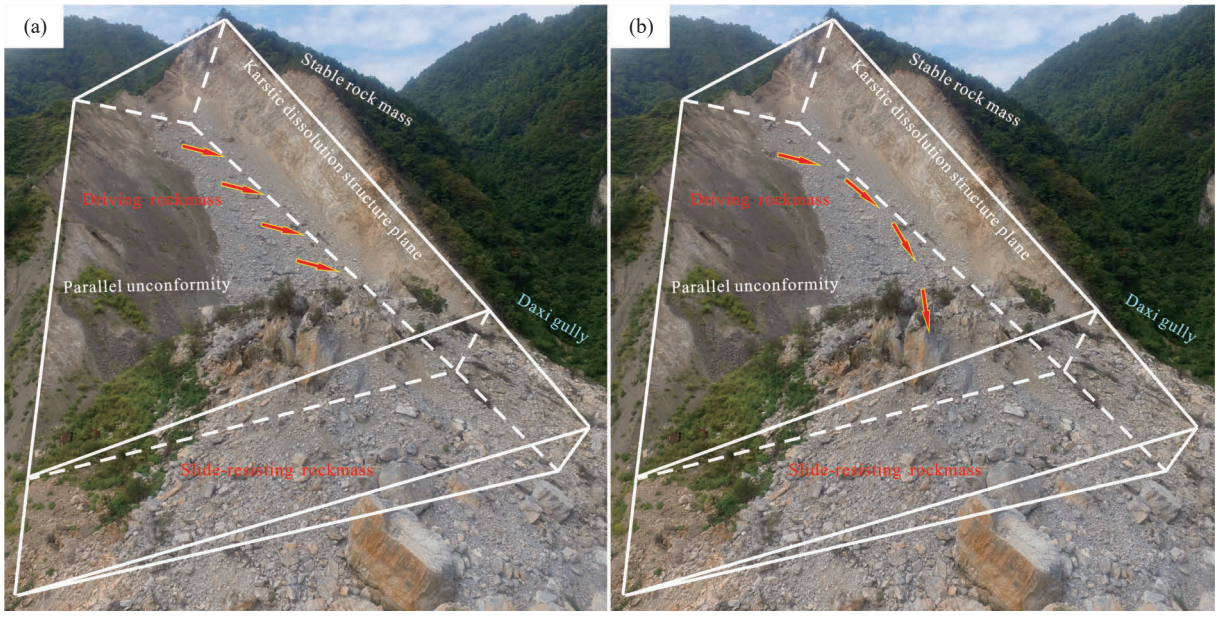

Fig. 15. Schematic diagram showing apparent dip creep-buckling of the Shanyang landslide. a–dip creeping; b–apparent dip slide-buckling.

a conceptual model of apparent sliding for obliquely inclined bedding rock masses after analyzing the mechanisms of the Jiweishan landslide, emphasizing the crucial role of the lateral discontinuity plane in shifting the slide direction from true dip to apparent dip for an obliquely inclined bedding landslide. The simulation and analysis of the Shanyang landslide's failure processes highlight the significance of slide-resisting forces in stabilizing the landslide. These forces originate from

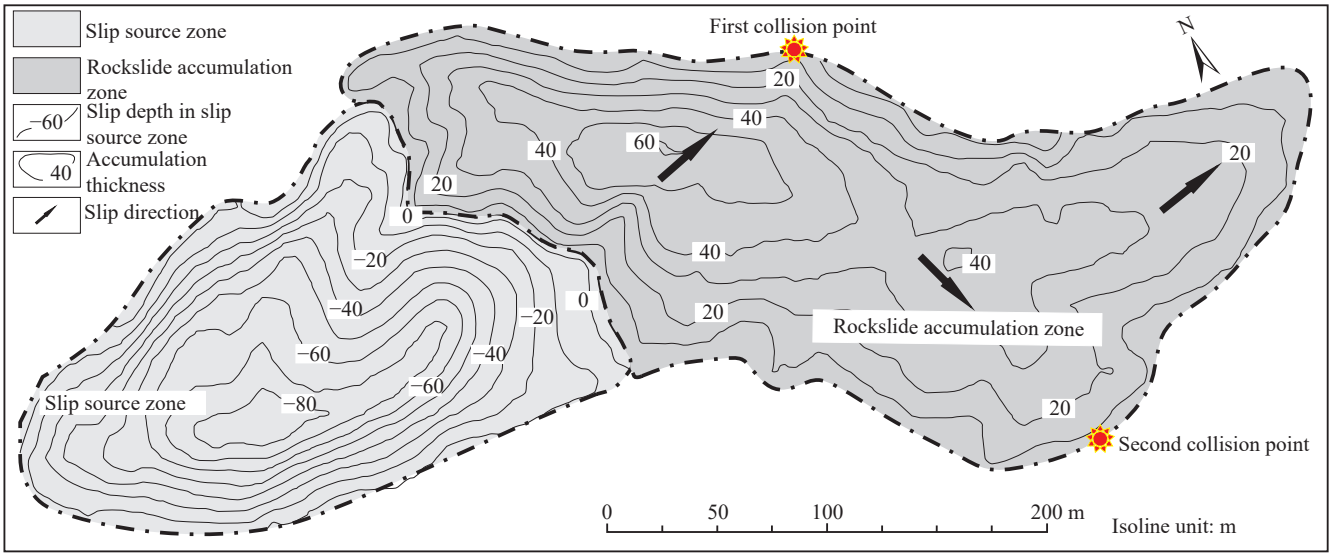

Fig. 16. Map showing the layout of the Shanyang landslide.

three sources: (1) The slide-resisting force on the slip surface due to the gravity of the sliding rock mass, (2) the slide-resisting force transmitted to the slide-resisting rock mass by the mountain slope's toe, and (3) the lateral friction force provided by the karstic dissolution structural plane. Among them, the last source is pivotal in the failure mechanism.

The physical and mechanical parameters of the dolomite in the numerical model are obtained through laboratory tests. But those of siliceous slate with carbonaceous mudstone in the numerical model are gotten according to the empirical parameters (Chang SP et al., 2006), and for the similarities in geological conditions of the Shanyang and Jiweishan landslides (Wang JY and Shi XY, 2018), the long-term strength and argillation strength of the carbonaceous mudstone are evaluated by using engineering geology analogy method according to Jiweishan landslide. So, the parameters used in the numerical model may differ somewhat from the actual. The lateral friction force, arising from discontinuities created by karstic dissolution, plays a pivotal role in the failure mechanism, but due to limited studies, the mechanism of lateral friction force on obliquely inclined bedding landslide has not been deeply studied, and further study is needed in the future. The rock slopes with obliquely inclined bedding structures are notably common in carbonate regions in southwestern China (Yin YP, 2008), and obliquely inclined bedding slopes with less visible apparent dip sliding are prone to undergo catastrophic geological events. Compared with the Jiweishan landslide, the Shanyang landslide, a hidden, apparent dip bedding slope, is governed by a subsurface weak interlayer at the slope's base. The higher dip angle and planar rotation angle in the Shanyang landslide resulted in a significant planar rotational slip, culminating in buckling failure in the front. So, the exploring the mechanism of hidden, steep obliquely inclined bedding landslides in this article has great significance for the identification, mechanism research and risk mitigation of obliquely inclined bedding landslide in southwestern China.

6. Conclusions

(i) The Shanyang landslide, occurring on a hidden, steep obliquely inclined bedding slope, manifests as apparent dip creep-buckling failure.

(ii) The weak interlayer underwent progressive argillization due to interlayer shear under the action of groundwater activity and the mountain slope's gravity, leading to the prolonged creep of the driving rock mass along a true dip angle. With the presence of the inclined stable rock mass barrier and the gradual decrease in lateral friction force due to karstic dissolution, the driving rock mass underwent planar rotation and slid along an apparent dip angle. The landslide ultimately resulted from the bending deformation and buckling failure of the slide-resisting rock mass.

(iii) The lateral friction force, arising from discontinuities created by karstic dissolution, plays a pivotal role in the failure mechanism behind the apparent dip creep-buckling in the steep obliquely inclined bedding landslide.

CRediT authorship contribution statement

Jia-yun Wang analyzed the field geological phenomena and investigated the failure process of the Shanyang landslide using 3DEC software. Zi-long Wu carried out the experiment and analyzed the data. Xiao-ya Shi analyzed the field geological phenomena and numerical simulation data. Long-wei Yang, Rui-ping Liu and Na Lu analyzed the test data and contributed to the interpretation of the results. All authors discussed the results and contributed to the final manuscript.

Declaration of competing interest

The authors declare no conflicts of interest.

Acknowledgment

This research was jointly supported by the projects of the China Geological Survey (DD20230092 and DD20201119).

The authors are indebted to Prof. Yue-ping Yin, Zhi-xin Chen, Dr. Sai-nan Zhu and Zhen Feng for their valuable advice and comments in this study.

References

AU SWC. 1998. Rain-induced slope instability in Hong Kong. Engineering Geology, 51(1), 1–36. doi: 10.1016/s0013-7952(98)00038-6.

Chang SP, Zhang SM. 2006. Handbook of Engineering Geology (fourth edition). Beijing, China Architecture and Building Press, 166–170 (in Chinese).

Cui FP, Xiong C, Wu Q, Xu C, Li N, Wu NA, Cui L. 2021. Dynamic response of the Daguangbao landslide triggered by the Wenchuan earthquake with a composite hypocenter. Geomatics Natural hazards & Risk, 12(1), 2170–2193. doi: 10.1080/19475705.2021.1944916.

Cundall PA, Hart RD. 1985. Development of generalized 2-D and 3-D distinct element programs for modeling jointed rock. ITASCA Consulting Group, Misc. Paper SL-85-1, U. S. Army Corps of Engeineers.

Cundall PA. 1971. The measurement and analysis of acceleration in rock slopes. London, University of London, Ph. D thesis, 1–130.

Cundall PA. 1980. UDEC-a generalized distinct element program for modeling jointed rock. Report PCAR-1-80, Peter Cundall Associates, European Research Office, U. S. Army, 1–80.

Huang RQ. 2007. Large-scale landslides and their sliding mechanisms in China since the 20th century. Journal Of Rock Mechanics And Geotechnical Engineering, 26, 433–454.

Hungr O, McDougall S. 2009. Two numerical models for landslide dynamic analysis. Computers & Geosciences, 35(5), 978–992. doi: 10.1016/j.cageo.2007.12.003.

Kutte HK. , Müller L. Translated by Li SP, Feng ZH. 1981. Rock mechanics. Beijing, China Coal Industry Publishing House, 1–330 (in Chinese).

Liu CZ, Shi T, Zhang MX. 1995. On the mechanism of deforming —cracking on the segment of cracks T8-T12 of Lianzi cliff dangerous rock body. Journal of Engineering geology, 3(2), 29–41 (in Chinese with English abstract). doi: CNKI:SUN:GCDZ.0.1995-02-003.

Mu JQ, Li TT, Pei XJ, Huang RQ, Lan FA, Zou XQ. 2022. Evolution mechanism and deformation stability analysis of rock slope block toppling for early warnings. Natural Hazards, 114(2), 1171–1195. doi: 10.1007/s11069-022-05422-8.

Pastor M, Haddad B, Sorbino G, Cuomo S, Drempetic V. 2009. A depth-integrated, coupled SPH model for flow-like landslides and related phenomena. International Journal for Numerical and Analytical Methods in Geomechanics, 33(2), 143–172. doi: 10.1002/nag.705.

Pipatpongsa T, Fang K, Leelasukseree C, Chaiwan, A. 2022. Stability analysis of laterally confined slope lying on oblique inclined bedding plane. Landslides, 19(8), 1861–1879. doi: 10.1007/s10346-022-01873-z.

Qiu P, Long Y, Zhang J. 2023. Research on deformation failure mechanism and stability of bedding cataclastic rock slope containing multi-muddy interlayers. Applied Sciences, 13, 8459. doi: 10.3390/app1314845.

Rahman AU, Zhang G, A AlQahtani S, Janjuhah HT, Hussain I, Rehman HU, Shah LA. 2023. Geotechnical assessment of rock slope stability using kinematic and limit equilibrium analysis for safety evaluation. Water, 15, 1924. doi: 10.3390/w15101924.

Sassa K. 1988. Geotechnical model for the motion of landslides //AA Balkema. Proceedings of the 5th International Symposium on Landslide. Rotterdam, 37–55.

Schuster RL, Lynn MH. 2001. Socioeconomic impacts of landslides in the Western Hemisphere. Reston, VA, USA, United States Geological Survey.

Sun GZ, Zhang WB. 1985. A commonly- sighted rock mass structure-slab-rent structure and its mechanical model. Chinese Journal of Geology, (3), 275–282 (in Chinese with English abstract).

Sun GZ. 1988. Structure mechanics of rock mass. Beijing, Science Press, 1–396 (in Chinese).

Wang J, Wang G, Shi X. 2019. Mechanical analysis of apparent dip creep-buckling failure of Shanyang Super large-scale rockslide in Shaanxi Province. Geology in China, 46(2), 381–388 (in Chinese with English abstract). doi: 10.12029/gc20190214.

Wang JY, Shi XY, Wu L, Zheng DG. 2018. Formation mechanism of apparent dip sliding in the Shanyang “8. 12” landslide. Northwestern Geology, 51(3), 232–239 (in Chinese with English abstract).

Wang JY, Shi XY. 2018. Mechanical analysis of apparent dip buckling mechanism of steep stratified oblique rock: A case study of Shanyang rockslide in Shaanxi Province. Journal of Geomechanics, 24(4), 582–489 (in Chinese with English abstract). doi: 10.12090/j.issn.1006-6616.2018.24.04.050.

Wang RQ, Zheng Y, Chen CX, Zhang W, Sun CY. 2023. Stability analysis of antidip bedding rock slopes with very low-persistent cross joints using a limit-equilibrium model and fracture mechanics. International Journal of Geomechanics, 23(5), 1–12. doi: 10.1061/ijgnai.gmeng-8151.

Xiong X, Matsumoto T, Shi Z, Zhang F. 2022. Flume tests and corresponding numerical simulation of hydraulic/mechanical behavior of Tangjiashan landslide dam subjected to seepage loading. Soils and Foundations, 62(5), 1–21. doi: 10.1016/j.sandf.2022.101200.

Xu B, Liu XR, Zhou XH, Guo XY, Wang Y, Huang JH, Liu J, Xiong F, Zhang JL. 2022. Investigation on the dynamic cumulative damage mechanism and stability of bedding rock slope under the deterioration of rock mass in the hydro-fluctuation belt. Bulletin of Engineering Geology and the Environment, 81(8), 1–23. doi: 10.1007/s10064-022-02833-6.

Yan GQ, Yin YP, Huang BL, Zhang ZH, Zhu SN. 2019. Formation mechanism and characteristics of the Jinjiling landslide in Wushan in the Three Gorges Reservoir region, China. Landslides, 16(11), 2087–2101. doi: 10.1007/s10346-019-01234-3.

Yang C, Shi W, Qian X, Peng X. 2023. Deformation and failure mechanism of bedding slopes induced by underground mining: Case study from Yanwan Village, Guizhou Province, China. Geotechnical and Geological Engineering, 41(3), 1877–1891. doi: 10.1007/s10706-023-02377-w.

Yang L, Wang W, Zhang N, Wei Y. 2020. Characteristics and numerical runout modeling analysis of the Xinmo landslide in Sichuan, China. Earth Sciences Research Journal, 24(2), 169–181. doi: 10.15446/esrj.v24n2.78990.

Yin Y, Sun P, Zhang M, Li B. 2011. Mechanism on apparent dip sliding of oblique inclined bedding rockslide at Jiweishan, Chongqing, China. Landslides, 8(1), 49–65. doi: 10.1007/s10346-010-0237-5.

Yin Y, Li B, Gao Y, Wang W, Zhang S, Zhang N. 2023. Geostructures, dynamics and risk mitigation of high-altitude and long-runout rockslides. Journal of Rock Mechanics and Geotechnical Engineering, 15(1), 66–101. doi: 10.1016/j.jrmge.2022.11.001.

Yin Y, Wang W, Zhang N, Yan J, Wei Y. 2017. The June 2017 Maoxian landslide: Geological disaster in an earthquake area after the Wenchuan Ms 8. 0 earthquake. Science China (Technological Sciences), 60, 1762–1766. doi: 10.1007/s11431-017-9148-2,.

Yin YP. 2008. Typical Landslides in China. Beijing, China Land Press, 1–198 (in Chinese).

Yin YP. 2010. Mechanism of apparent dip sliding of oblique inclined bedding rockslide—a case study of Jiweishan rockslide in Wulong, Chongqing. Chinese Journal of Rock Mechanics and Engineering, 19(2), 217–226 (in Chinese with English abstract). doi: 10.1016/S1876-3804(11)60004-9.

Zhang Y, Xing A, Li B, Bilal M, Chang W. 2023. Two-dimensional frictional heating simulation based on landslide process reconstruction. Landslides, 20(11), 2303–2315. doi: 10.1007/s10346-023-02113-8.

Zou ZX, Tang HM, Xiong CR, Su AJ, Criss RE. 2017. Kinetic characteristics of debris flows as exemplified by field investigations and discrete element simulation of the catastrophic Jiweishan rockslide, China. Geomorphology, 295, 1–15. doi: 10.1016/j.geomorph.2017.06.012.